Journal of Mines, Metals and Fuels, *73(8): 2579-2590; 2025. DOI: 10.18311/jmmf/2025/49334*

Print ISSN : 0022-2755

Journal of Mines, Metals and Fuels

Contents available at: *www.informaticsjournals.co.in/index.php/jmmf*

Fatigue Life Prediction and Optimization of AA2219 Using Taguchi and Regression Analysis

Madhukar Samatham[1], S. Chandra Sekhar[2]*, C. Naga Kumar[3], Bana Veerendra[4], G. Suresh Babu[5] and P. Saritha[6]

[1]*Department of Mechanical Engineering, Lords Institute of Engineering and Technology, Himayath Sagar, Hyderabad - 500086 Telangana, India*

[2]*Department of Mechanical Engineering, N. B. K. R Institute of Science and Technology (Autonomous), Vidyanagar, Tirupati – 524413, Andhra Pradesh, India; chanduskr1988@yahoo.com*

[3]*Department of Mechanical Engineering, G. Pullaiah College of Engineering and Technology, Kurnool - 518452, Andhra Pradesh, India*

[4]*Department of Mechanical Engineering, Rajeev Gandhi Memorial College of Engineering and Technology, Nandyal - 518501, Andhra Pradesh, India*

[5]*Department of Mechanical Engineering, Annamacharya University, Rajampet - 516126, Andhra Pradesh, India*

[6]*Department of Mechanical Engineering, School of Engineering, Anurag University, Hyderabad - 501301, Telangana, India*

Abstract

In the present study, the fatigue life of aerospace-grade AA2219 aluminium alloy was systematically evaluated under varying cyclic loading conditions using a combined Taguchi experimental design and regression analysis. AA2219, widely deployed in cryogenic tanks and structural aerospace components, exhibits sensitivity to fatigue damage due to its precipitation-hardened microstructure. A two-factor, three-level Taguchi L9 orthogonal array was implemented, considering maximum stress level and loading frequency as critical input parameters. Experimental fatigue tests were conducted per ASTM E466, and the resulting fatigue lives were analysed through ANOVA to identify dominant influencing factors. The maximum stress level emerged as the most significant factor, contributing 6.83% to fatigue life variation, while loading frequency exhibited a secondary effect. A second-order polynomial regression model was developed and validated, exhibiting excellent accuracy with an R^2 of 0.9997 and RMSE of 183.86. SEM-based fractography confirmed distinct fatigue mechanisms under low and high stress regimes, including striation development and brittle fracture morphologies. A confirmation experiment demonstrated only 2.15% deviation between predicted and experimental fatigue life, validating the model's reliability. The proposed methodology offers a predictive and optimization framework to enhance the fatigue performance of AA2219, reducing experimental workload while providing actionable insights for aerospace structural design.

Major Findings: *Maximum stress level emerged as the key parameter influencing fatigue life, contributing 6.83% to the total variation observed. A robust second-order regression model (R^2 = 0.9997) was developed, predicting fatigue life with only a 2.15% deviation from actual experiments, proving its reliability. SEM-based fractographic analysis revealed a clear transition: fine fatigue striations dominated at low stress, while brittle, quasi-cleavage features took over at higher stresses.*

Keywords: *AA2219, Fatigue Life Prediction, Fractographic Analysis, Regression Analysis, Taguchi Method*

**Author for correspondence*

1.0 Introduction

Lightweight high strength materials play a crucial role in aerospace and high-performance structural systems because they enable better payload efficiency and structural integrity and improved fuel economy. The development of advanced aluminium alloys represents the primary solution for next generation aerospace engineering because they provide superior strength-to-weight ratio and thermal resilience. AA2219 demonstrates excellent weldability and mechanical durability at high temperatures[1]. It provides excellent strength together with corrosion resistance and thermal endurance for aerospace applications mainly in cryogenic fuel tanks and fuselage frames and launch vehicle structural components[2,3]. AA2219 demonstrate a unique microstructural behaviour characterized by a robust precipitation hardening mechanism that enhances its strength[4]. The fine precipitates in this alloy are distributed uniformly that contribute to improved thermal stability during prolonged exposure to high temperatures. AA2219 is susceptible to microstructural evolution under cyclic loading and thermal stress that include precipitate coarsening and phase transformations which could subtly alter its mechanical properties[5,6].

Microstructural enhancements in recent years of 2xxx series Al-Li alloys have resulted in consistent advancements in their fatigue and damage tolerance characteristics. Kermanidis *et al.,*[7] investigated the fatigue and damage tolerance of the alloy under various artificial ageing conditions, revealing that the conventional yield stress Rp0.2% increased by over 50%, 46% reduction in tensile ductility Af and a 44% decrease in the critical stress intensity factor. Wang *et al.,*[8] investigated the impact of pre-deformation and levels prior to artificial aging on the microstructural development and Fatigue Crack Growth (FCG) behaviour of Al-Cu-Li-Sc alloy sheets. It was found that the pre-stretching level increased from 1% to 4.5% and FCG rate first decreased and then increased at a stress intensity factor range (ΔK) of 20 MPa·$m^{1/2}$. The HCF behaviours of cast aluminium alloys at room temperature and elevated temperatures were investigated by Liang *et al.,*[9] and it was observed that the fatigue life decreased significantly at 300 ℃ as compared to room temperature. The fracture analysis showed that pores are the primary sites for crack nucleation at room temperature as well as at 200 ℃, and cracks also nucleate from hard particles and slip bands at 300 ℃ due to the presence of multiple nucleation sites. Sreearravind *et al.,*[10] assessed the impact of Equal Channel Angular Pressing (ECAP) on the mechanical characteristics and fatigue behaviour of aluminium 6063 at channel angles of 90° and 120°, with a curvature radius of 20° at the room temperature. Stress-strain hysteresis investigation indicated stable modulus ratios of around 1.006 - 1.007 for ECAP samples, with low plastic strain amplitudes of 0.001% that indicate effective resistance to cyclic deformation. Yang *et al.,*[11] examined the mechanical characteristics of 2017 aluminium alloy produced using CCDR at high temperatures and cyclic heating-cooling conditions and found that the high temperature solution treatment led to grain coarsening and precipitation that adversely affected the fatigue life, and the ductility progressively reduced after 500 thermal fatigue cycles.

Predicting the fatigue lifespan of aluminium alloys like AA2219 under variable amplitude and cyclic loading conditions continues to be a significant problem because of the intricate stress interactions, microstructural alterations, and nonlinear damage. The transition between Low Cycle Fatigue (LCF), typically characterized by high strain amplitudes and limited life cycles ($<10^4$-10^5 cycles), and High Cycle Fatigue (HCF), involving lower strain amplitudes with life cycles exceeding 10^5, stands as a critical point where fatigue damage builds from elastic along with plastic deformations[12]. Specific characterization of this transition stands essential because it affects both the structural reliability and service life of components experiencing mixed loading conditions with LCF and HCF mechanisms active simultaneously[13,14]. Al-Cu series have been subject to considerable efforts over years toward understanding the fatigue behaviour of them because of their critical application in aerospace structures. The traditional methods of predicting fatigue utilize S-N (stress life)[15,16] and ε-N (strain life)[17] approaches with empirical data obtained from controlled laboratory testing. It is evidenced that fatigue behaviour of AA2219 under variable amplitude loading is very sensitive to microstructural factors like precipitate distribution, grain size and residual stresses[18]. Studies using constant amplitude loading have produced basic fatigue data[19]. The study of thermal exposure in cryogenic and extreme temperature conditions has been done to explore its effect on cyclic life and the processes of initiation of damage[20,21]. Notwithstanding these basic efforts, the natural

nonlinearity and stochastic nature of fatigue degradation in AA2219 in the transition zone between LCF and HCF cause inaccuracies in forecasting.

The S-N technique is often the most appropriate for the preliminary design phase of bonded structures, because of its simplicity and comprehensive analysis of total fatigue life. Sousa *et al.*,[22] combined hydrostatic and deviatoric strain energy density components with the notion of critical distances to formulate a cohesive fatigue life prediction approach for homogeneous and heterogeneous composite and metal adhesive connections. Deng *et al.*,[23] established a life prediction model for gears utilizing the dislocation energy method in conjunction with the fatigue failure mechanism. Their findings indicated that the fatigue reliability of gears reduces not only with the increase of the operating parameters but also exhibits a declining trend over time. Qianyu *et al.*,[24] adopted the Continuum Damage Mechanics-Finite Element Method (CDM-FEM) using a Particle Swarm Optimization (PSO) approach to forecast the Medium-Low-Cycle Fatigue (MLCF) life of perforated structures. Reinforcement of cross-sections and cold expansion in engineering may significantly enhance the fatigue lifespan of perforated structures.

Extensive research has been performed on the fatigue characteristics of Al-Cu alloys yet successful prediction of fatigue life under variable amplitude loading remains challenging. Most prior studies have predominantly relied on empirical S-N or strain-life approaches based on conventional fatigue testing under constant amplitude loading. The existing methods fail to adequately capture the complex nonlinear damage accumulation processes that require optimized statistical modeling approaches. Taguchi design and regression analysis are chosen due to their demonstrated efficacy in efficient identifying significant factors, optimize parameter combinations, and provide statistically reliable predictive equations for engineering applications. The present work uniquely integrates a Taguchi-based design of experiments to efficiently identify critical fatigue-influencing factors and develops a regression-based analytical model to generalize fatigue life behavior under varying cyclic loading conditions. By adopting this combined statistical modeling and optimization approach, the study deviates from traditional empirical practices and offers a predictive framework that is inherently more adaptable for engineering design applications.

The aim of the present study is to evaluate the fatigue properties of AA2219 through a structured Taguchi experimental design and investigate the important influencing parameters. This is achieved by developing a reliable regression-based fatigue life prediction model to predict its performance under different cyclic loading conditions and perform constrained optimization to determine operating conditions that optimize fatigue life through Analysis of Variance (ANOVA) and determine individual factor and interaction effects.

2.0 Material and Methods

2.1 Material

AA2219 is a high-strength, precipitation-hardened aluminum-copper alloy, widely used in aerospace

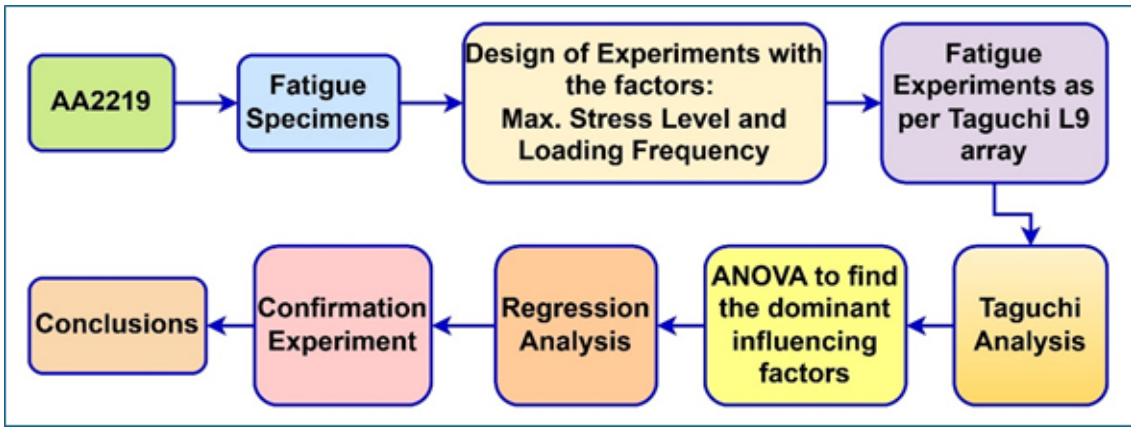


Figure 1. Flowchart of the work undertaken.

Table 1. Chemical composition (wt. %)

Element	Cu	Fe	Mn	Si	Ti	V	Zr	Al
Composition (%)	6.2	0.22	0.25	0.18	0.03	0.1	0.16	Balance

applications for its excellent weldability, high-temperature performance, and fatigue resistance. It is solution-treated, cold-worked, and artificially aged to optimize its mechanical properties[25]. However, predicting its fatigue life under varying loading conditions remains a critical challenge for ensuring structural reliability especially in the transition zone from low-cycle fatigue to high-cycle fatigue. The chemical composition (from Spark Optical Emission Spectrometry) of the alloy are presented in Table 1.

2.2 Fatigue Testing

Figure 2 shows the drawing of the fatigue specimens designed as per ASTM E466 standard and Figure 3 presents the fabricated specimens.

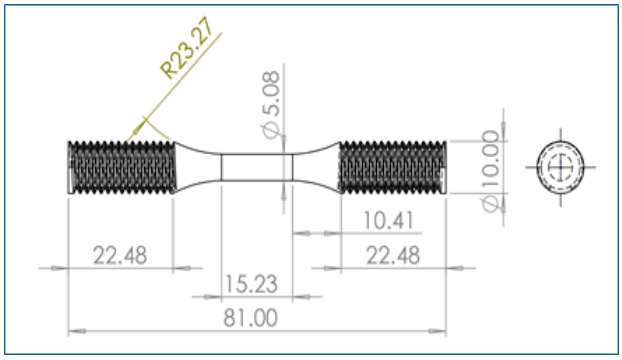


Figure 2. Drawing of the ASTM E466 fatigue specimen.

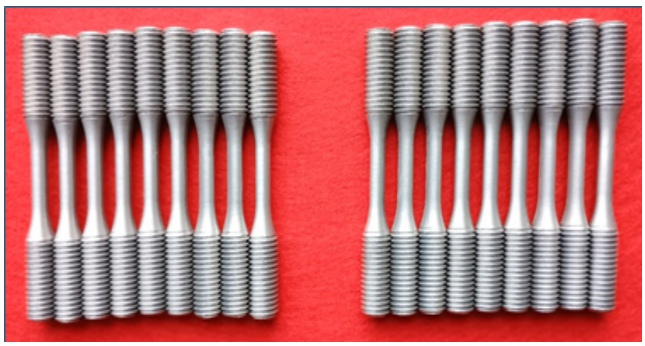


Figure 3. Fatigue specimens after fabrication (left: trial; right: trial 2)



Figure 4. Fatigue testing machine.

Experimental fatigue testing was carried out on a 25kN Nano UTM (Make: ITW – BISS) with servo hydraulic control. It is a computer-controlled machine with fatigue accessories, extensometers and data acquisition system. The machine supports total stress-control and total strain-control fatigue testing methodologies. Total stress control experimental runs were conducted at room temperature for the present research and Figure 4 illustrates the FTM employed.

2.3 Experimental Design

Table 2 presents the factors and their levels chosen for the present research. Quantification of the impact of the factors on the response which is fatigue life (Y) in cycles is performed, and optimal parameters condition is identified from Taguchi analysis. Thereafter, regression analysis is

Table 2. Details of factors and their levels

S. No	Factor	Notation	Units	Low	Medium	High
1	Maximum Stress Level	X1	MPa	320	330	340
2	Loading Frequency	X2	Hz	8	10	12

performed to develop a prediction model for the response. The regression equation is then subjected to constrained optimization to find the optimal condition. The deviation between the two optimal conditions (Optimal conditions from Taguchi and Regression analysis) is then found. The percentage contribution of the factors to the response is also computed from ANOVA to find the significance of each factor. The L_9 array is represented in Table 3.

Table 3. Taguchi L9 array

Run	X1	X2
1	320	8
2	320	10
3	320	12
4	330	8
5	330	10
6	330	12
7	340	8
8	340	10
9	340	12

2.4 Scanning Electron Microscopy

Scanning Electron Microscopy (SEM) was undertaken to examine the fractographic characteristics of the fatigue failed specimens. The S-3700N machine from hitachi high-technologies corporation was used to capture high-resolution images of the surfaces and layer adhesion. A focused electron beam interacted with the sample, generating secondary electrons to reveal the modes of failure.

2.5 Analysis of Variance

To statistically compute the relative contribution of input variables toward the fatigue life of AA2219, a comprehensive ANOVA was conducted using the polynomial regression model as the foundational structure. ANOVA aids in parsing the total observed variability in fatigue life into quantifiable segments attributed to individual parameters (main effects), their higher-order terms (nonlinear effects), and their combined interactions. In this study, ANOVA deconstructs the variance into six distinct sources: the main effects of maximum stress level (X1) and loading frequency (X2), their squared terms ($X1^2$, $X2^2$), their interaction (X1.X2), and the residual error.

3.0 Results and Discussion

3.1 Fatigue Results

Table 4 presents the experimentally recorded fatigue lives (in cycles) of AA2219 under nine distinct combinations of maximum stress level and loading frequency, following the Taguchi L_9 orthogonal array design. Each condition was tested at least twice to ensure repeatability, and the average value of the two best trials is reported as the fatigue life for a given run. A clear and consistent trend emerges across the data: as the maximum stress level increases from 320 MPa to 340 MPa, the fatigue life (Y) significantly decreases, irrespective of the loading frequency. For instance, at 320 MPa and 8 Hz (Run 1), the average fatigue life was approximately 26,721 cycles, whereas at 340 MPa and the same frequency (Run 7), it dropped sharply to 12,681 cycles, a reduction of over 50%. This trend confirms the expected inverse relationship between applied stress and fatigue durability. Furthermore, an increase in loading frequency (X_2) from 8 Hz to 12 Hz at any constant stress level also correlates with a drop in fatigue life. At 320 MPa, increasing the frequency from 8 Hz (Run 1) to 12 Hz (Run 3) results in a fatigue life reduction from 26,721 to 23,491 cycles. A similar degradation pattern is observed at 330 MPa and 340 MPa levels as well. Collectively, the data reflects a synergistic degradation of fatigue performance under the combined influence of higher stress and increased loading frequency. These experimental insights set the foundation

Table 4. Fatigue results in cycles

Run	X1	X2	Y (cycles)		
			Trial 1	Trial 2	Average
1	320	8	26899	26543	26721
2	320	10	25917	25207	25562
3	320	12	23327	23654	23491
4	330	8	16475	16992	16734
5	330	10	15236	14876	15056
6	330	12	13548	13102	13325
7	340	8	12585	12776	12681
8	340	10	11326	11839	11583
9	340	12	9345	9984	9665



Figure 5. Fatigue specimen of run 1 post failure.

for deeper statistical treatment via Taguchi analysis and regression modeling, which will subsequently identify the optimal conditions that maximize fatigue life while quantifying the contribution of each factor. The fatigue specimen of Run 1 after failure is presented on a sampling basis in Figure 5.

Figure 6 illustrates the variation in average fatigue life of AA2219 as a function of two critical parameters: maximum stress level and loading frequency. The slope of the fatigue decline becomes increasingly steep as stress levels rise, indicating a nonlinear degradation pattern, particularly pronounced at 330 MPa and above. Additionally, the frequency effect, while secondary, reveals a consistently downward trend, suggesting that elevated cyclic rates may accelerate crack propagation by reducing the time available for local plastic redistribution at crack tips[12-26]. These graphical insights reinforce the understanding that maximum stress level is the dominant factor, but its interaction with frequency cannot be overlooked. The fatigue behaviour shown in Figure 6 provides a visual confirmation of the tabular data and lays a foundational basis for subsequent statistical modelling and optimization strategies.

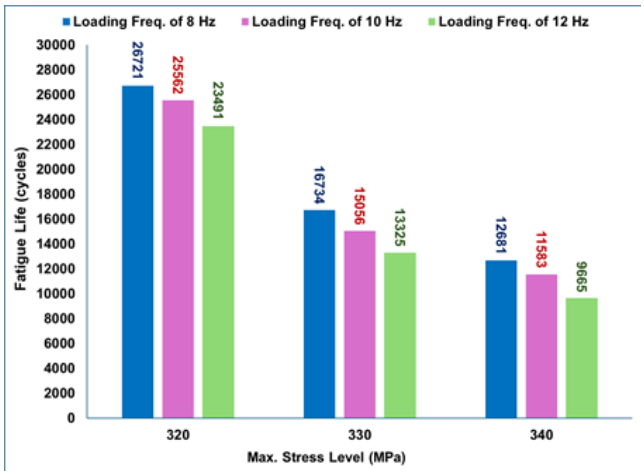


Figure 6. Trends of fatigue lives at different factors.

3.2 SEM Analysis

The SEM-based fractographic image corresponding to Run 1, characterized by a maximum stress of 320 MPa and a loading frequency of 8 Hz, as shown in Figure 7, reveals classic features of fatigue failure initiated under low-stress, high-life conditions. The fracture surface exhibits a well-defined crack initiation zone along the outer periphery, typically originating from the surface, which is a common feature in high-cycle fatigue where surface flaws or stress concentrators act as primary initiation sites[26,27]. A series of concentric beach marks or striations are clearly visible, indicating progressive crack growth under cyclic loading. These marks serve as chronological evidence of stable crack advancement, controlled by localized plastic deformation[28]. The spacing between striations

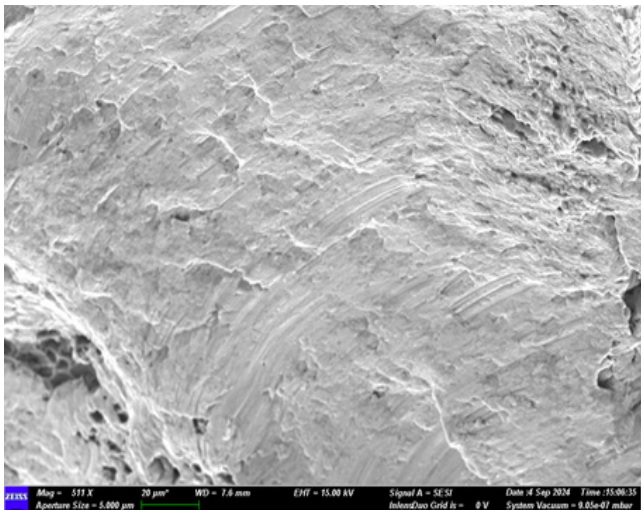


Figure 7. Fractography of run 1.

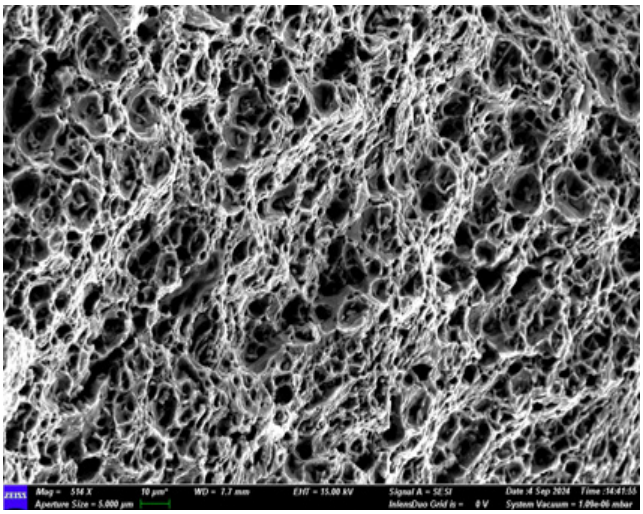


Figure 8. Fractography of run 9.

appears uniform and widely spaced, consistent with the relatively low stress intensity and the extended number of load cycles endured by the material before failure[29]. In the final fracture region, the morphology transitions into a dimpled rupture zone, characteristic of micro-void coalescence and ductile overload. This transition confirms that the crack propagated slowly over time and culminated in a sudden final fracture once the remaining cross-section could no longer sustain the applied load[30].

The SEM-based fractographic analysis of Run 9, conducted under the most aggressive loading condition (340 MPa, 12 Hz), as shown in Figure 8, reveals a markedly different failure morphology compared to low-stress conditions. The fracture surface is indicative of a Low-Cycle Fatigue (LCF) regime dominated by accelerated crack initiation and unstable crack growth, consistent with the significantly reduced fatigue life recorded[31]. Unlike run 1, where striations and beach marks were prominent, the surface of Run 9 displays a coarser texture with fewer discernible striations, suggesting rapid crack propagation with limited time for crack tip blunting. The initiation site remains surface-originated, but the propagation zone appears more chaotic and lacks the uniformity typically seen in high-cycle fatigue[32]. This is suggestive of microstructural damage accumulation at a faster rate, likely driven by the elevated cyclic stress and reduced relaxation time between cycles due to the higher frequency[3,33]. Toward the final fracture region, the surface transitions into areas exhibiting quasi-cleavage and intergranular features, pointing toward a mixed-mode failure, predominantly brittle in nature, with localized plastic deformation[19,26]. The presence of flat facets and river patterns in some regions corroborates this brittle character, indicating that the material fractured before significant plastic accommodation could occur[20].

3.3 Taguchi Analysis

ANOM plot Figure 9 serves as a powerful diagnostic tool in the Taguchi framework to identify the most influential parameters and the direction in which they affect the response variable. The plot distinctly highlights that maximum stress level exerts the most substantial

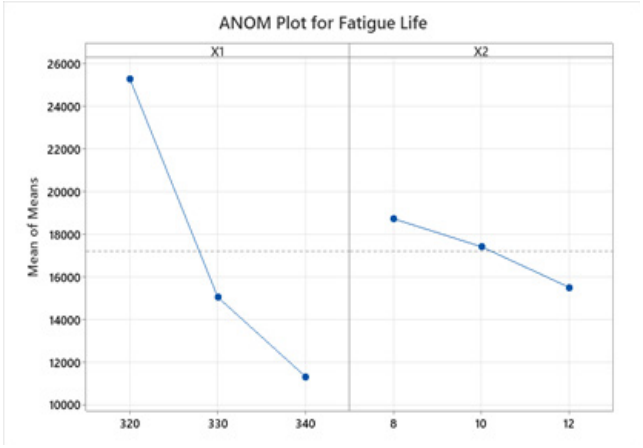


Figure 9. ANOM plot for fatigue life.

impact on fatigue life. As it increases from 320 MPa to 340 MPa, a sharp and nearly linear drop in average fatigue life is observed. This is consistent with the physical understanding that higher stress amplitudes accelerate crack initiation and growth, thereby reducing fatigue endurance[34]. In contrast, loading frequency exhibits a milder but consistent downward trend in fatigue life as the frequency rises from 8 Hz to 12 Hz. This behaviour suggests that increased cyclic rates reduce the material's ability to undergo local plastic relaxation at the crack tip, leading to premature failure[35]. The optimal condition inferred from the ANOM plot are X1 = 320 MPa and X2 = 8 Hz and this correlates with the experimental data Table 4.

3.4 Regression Analysis

Regression analysis is carried out using MiniTab package and the polynomial regression equation of fatigue life (Y) in terms of the two factors is as follows:

$$Y = 3789170 - 22144\,X1 - 200\,X2 + 32.46\,X1*X1 - 74.4\,X2*X2 + 2.68\,X1*X2 \quad (1)$$

The RMSE (183.86) and R-squared (0.9997) values indicate both the accuracy and generalizability of the developed equation. To re-verify the robustness of the regression equation, it is subjected to constrained maximization using MATLAB within the boundaries of 320<=X1<=340 and 8<=X2<=12. As expected, the optimal values of the factors that maximize the fatigue life (Y) within the given bounds are: X1= 320 MPa, X2= 8 Hz and the predicted fatigue life is 27,493 cycles. The percentage difference between the actual fatigue life (26,721 cycles) from Table 4 and the predicted fatigue life (27,493 cycles) from Equation 1 is mere 2.89% and this proves the robustness of the equation developed. Equation 1 can efficiently replace experimental fatigue runs within the boundaries of the maximum stress level and loading frequencies chosen in the present work. This makes the lives of engineers and scientists easy as the costly and cumbersome activity of experimental fatigue runs is replaced with mathematical formulation.

3.5 ANOVA

The ANOVA results Table 5 provide quantitative insight into the contribution of each factor and interaction on the fatigue life of AA2219. Maximum stress level (X1) emerges as the most influential factor, contributing 6.83% to the total variation. Its squared term (X1*X1) also contributes significantly (6.41%), indicating a strong nonlinear effect of stress on fatigue behaviour. Conversely, loading frequency (X2) has a negligible impact, contributing just 0.0002%, and its squared term adds only 0.054%, which highlights its secondary role in comparison to stress. The interaction term (X1*X2) contributes merely 0.0034%, confirming that the combined effect of stress and frequency on fatigue life is minimal within the tested domain.

Table 5. ANOVA results

Source	DF	SS	MS	p-value	% Contribution
Regression	5	328625510	65725102		--
X1	1	22448895	22448895	0.000	6.8300
X2	1	495	495	0.911	0.0002
X1*X1	1	21066541	21066541	0.000	6.4100
X2*X2	1	177012	177012	0.106	0.0540
X1*X2	1	11449	11449	0.601	0.0034
Error	3	101412	33804		--
Total	8	328726922	--		--

The model residual (Error) remains exceptionally low (0.03%), indicating a high level of experimental accuracy and a well-fitting regression model. These results validate the dominance of stress-level-dependent mechanisms in governing fatigue life, and they justify the emphasis on optimizing X_1 over X_2 during fatigue life enhancement strategies[36].

3.6 Confirmation Experiment

A confirmation experiment was carried out at new values of X1 and X2 to perform a comparative analysis of the predicted fatigue life with that of the experimental fatigue life Table 6.

Table 6. Comparative analysis of predicted (vs) confirmation experimental fatigue life

X1	X2	$Y_{Predicted}$ (Regression)	Y_{actual} (Experiment)	% Deviation
335	11	12,497	12,234	2.15

The percentage deviation of 2.15% between predicted and actual fatigue life confirms the model's reliability and generalizability within the operational domain. This minor deviation not only reinforces the robustness of the developed regression equation but also demonstrates its practical utility in reducing the dependency on extensive fatigue testing, especially when exploring fatigue response in interpolated or extrapolated design conditions[37]. Such predictive capability is indispensable for aerospace design workflows where time, cost, and material constraints limit exhaustive experimentation.

4.0 Conclusions

This study investigated the fatigue behaviour of AA2219 aluminium alloy under varying cyclic loading conditions using a combination of Taguchi experimental design, regression analysis, and SEM-based fractographic examination. The approach not only enabled the identification of statistically significant parameters influencing fatigue life but also facilitated the development of a robust predictive model to reduce experimental burden in future design scenarios. The integration of experimental and statistical tools provides a holistic framework for understanding fatigue mechanisms in aerospace-grade materials.

Key findings of the study are as follows:

- The maximum stress level is the most critical parameter influencing fatigue life, contributing 6.83% to the total variance, while loading frequency played a secondary role.
- A second-order regression model was developed with an exceptionally high coefficient of determination (R^2 = 0.9997) and a low RMSE of 183.86 cycles, indicating strong predictive capability within the tested domain.
- A confirmation experiment showed only 2.15% deviation from the predicted fatigue life, supporting the model's accuracy and generalizability.
- SEM fractography revealed a transition from well-defined fatigue striations at low stress (high-cycle fatigue regime) to quasi-cleavage and brittle fracture morphologies at high stress, corroborating mechanical findings.

In summary, this work delivers a practical and statistically validated methodology for fatigue life prediction and optimization in AA2219 alloy. The developed framework offers substantial potential for reducing experimental fatigue testing and guiding aerospace component design. Despite the high predictive accuracy of the developed regression model, certain inherent limitations must be acknowledged. First, the model is based on uniaxial cyclic loading conditions and does not account for multiaxial stress states that components often experience in service. Second, the influence of material anisotropy, a known characteristic of rolled and aged AA2219, was not explicitly considered, although it can significantly affect fatigue crack initiation and propagation behavior. Third, surface finish effects, such as roughness or machining marks, were not parameterized in the current study, although they are critical fatigue life determinants. These simplifications, while enabling a focused analysis, may restrict direct extrapolation to complex real-world aerospace structures without appropriate calibration. Future studies should address these factors to enhance the model's practical applicability. The predictive framework developed herein can be significantly enhanced by integrating advanced Machine Learning (ML) and surrogate modeling approaches. Techniques such as Gaussian Process

Regression (GPR), Artificial Neural Networks (ANNs), or Support Vector Regression (SVR) could be deployed to model complex nonlinear interactions between stress, frequency, microstructural features, and fatigue life with greater flexibility than polynomial regression. Moreover, surrogate-based optimization methods could enable rapid fatigue life predictions across a broader range of design and environmental variables without extensive experimental testing. Incorporating ML algorithms trained on expanded datasets, possibly including microstructural descriptors and thermal history, could further improve the model's generalizability and predictive robustness, supporting accelerated material design and lifecycle management strategies for aerospace structures.

5.0 References

1. Tao H, Chang Z, Shen Y, Liu Z, Jiang B, Li Z, Cai Q, Zhang H. Optimization of microstructure and mechanical properties of 2219 Al alloy cold-sprayed coating by heat treatment. J Therm Spray Technol. 2025; 34:250-266. https://doi.org/10.1007/s11666-024-01914-0
2. Livatyali H, Keles O. Additive friction stir deposition for aluminum alloys in aerospace applications. Aluminum technologies in aerospace applications. Cham: Springer nature Switzerland; 2025. p. 149-188. https://doi.org/10.1007/978-3-031-82447-0_7
3. He W, Hu Y, Wu Z, Wang F, Meng F, Lin Y, Wang G, Wu S. Defect sensitivity and high-cycle fatigue resistance of arc-welded 2219 aluminum alloy at 77 K. Int J Fatigue. 2024; 182:108189. https://doi.org/10.1016/j.ijfatigue.2024.108189
4. Malayeri AN, Hanzaki ZA, Moshiri A, Abbasi A, Abedi HR. Heterogeneous microstructure enables strength-ductility synergy in 2219 aluminium alloy fabricated by Wire Arc Additive Manufacturing (WAAM). Progress in Additive Manufacturing. 2025. https://doi.org/10.1007/s40964-025-00985-x
5. Acquah E, Bhowmik S, Hossain AM, Kumar N. Stress corrosion cracking of AA7075 Aluminum alloy processed via additive friction stir deposition. J Mater Eng Perform. 2025. https://doi.org/10.1007/s11665-025-10738-0
6. Zeng X, Fan XG, Li HW, Zhan M, Li SH, Ren TW, Wu KQ. Grain refinement in hot working of 2219 aluminium alloy: on the effect of deformation mode and loading path. Materials Science and Engineering: A. 2020; 794:139905. https://doi.org/10.1016/j.msea.2020.139905
7. Kermanidis AT, Charalampidou CM, Goulas I, Skarvelis P, Alexopoulos ND. Fatigue and fracture behaviour of (Al-Cu-Li) AA2198 under different ageing conditions. Int J Fatigue 2024; 184:108286. https://doi.org/10.1016/j.ijfatigue.2024.108286
8. Wang P, Ye L, Li Z, Guo X, Tang J, Liu S, Zhang Y. Influence of pre-deformation on the fatigue crack propagation and fracture behaviour of Al-Cu-Li-Sc alloy. Theoretical and Applied Fracture Mechanics; 2025. p. 104913. https://doi.org/10.1016/j.tafmec.2025.104913
9. Liang Y, Zuo Z, Wang J, Zhao C, Ren P, Huang W. Study on high cycle fatigue behaviours and modelling of cast aluminium alloy at elevated temperatures. Engineering Failure Analysis. 2025; 168:109031. https://doi.org/10.1016/j.engfailanal.2024.109031
10. Sreearravind M, Ravisankar B, Kumar RS. Low cycle fatigue behaviour of aluminium 6063 alloy processed by equal channel angular pressing at 90° and 120° channel angles. Materials Today Communications. 2025; 42:111401. https://doi.org/10.1016/j.mtcomm.2024.111401
11. Yang CH, Huang BC, Zhao JR, Hung FY. Microstructure and high-temperature fracture mechanism of continuously cast and directly rolled 2017 Al-Cu Alloy. J Mater Eng Perform. 2025. https://doi.org/10.1007/s11665-025-10643-6
12. Dhanasekaran MP, Agilan M, Selvan SK, Swain D, Rao GS, Muthukumar R, Mahapatra DR. Effect of laser shock peening on local tensile behaviour of various zones of AA2219 friction stir weld. Materials Today Communications. 2025; 44:111999. https://doi.org/10.1016/j.mtcomm.2025.111999
13. Hussain G, Shehbaz T, Alkahtani M, Khaliq UA, Wei H. Nanomechanical, mechanical and microstructural characterization of electron beam welded Al2219-T6 tempered aerospace grade alloy: A comprehensive study. Heliyon. 2024; 10(1). https://doi.org/10.1016/j.heliyon.2023.e23835 PMid:38205289 PMCid:PMC10777004.
14. Ramachandra GS, Boppana SB, Dayanand S, Nagaral M, Auradi V. Microstructure, mechanical behaviour, and tensile fractography of Si3N4-Reinforced Al2219 alloy composites synthesized by squeeze casting method. J Fail Anal Prev. 2024; 24(4):1719-1729. https://doi.org/10.1007/s11668-024-01956-0

15. Owolabi GM, Thom M, Ajide O, Kumar N, Azimi A, Whitworth H, Warner G. Fatigue responses of three AA 2000 series aluminum alloys. J Mater Sci Chem Eng. 2019; 7(3):32-48. https://doi.org/10.4236/msce.2019.73003
16. Ganesan K, Rao TS, Rao SK. Investigating the effect of stress ratio on fatigue crack growth rate behaviour in friction stir welded AA7075-T651 aluminium alloy plates. Int J Fatigue. 2024; 188:108527. https://doi.org/10.1016/j.ijfatigue.2024.108527
17. Li K, He X, Li L, Yang L, Hu J. Residual stress distribution of aluminium-lithium alloy in hybrid process of friction stir welding and laser peening. Optics and Laser Technology. 2022; 152:108149. https://doi.org/10.1016/j.optlastec.2022.108149
18. Zhang D, Wang G, Wu A, Zhao Y, Li Q, Liu X, Meng D, Song J, Zhang Z. Study on the inconsistency in mechanical properties of 2219 aluminium alloy TIG-welded joints. Journal of Alloys and Compounds. 2019; 777:1044-1053. https://doi.org/10.1016/j.jallcom.2018.10.182
19. Wu Z, Wu S, He W, Meng F, Wang L, Wang F, Hou C, Wang G. X-ray tomography of failure behaviours of arc welded AA2219 joints under tensile and cyclic loading. Materials Characterization. 2023; 205:113311. https://doi.org/10.1016/j.matchar.2023.113311
20. Hu Y, Wu S, Wang Z, Meng F, Xue Y, Fu Y, Kang G, Withers PJ. Void nucleation and growth behaviour of TIG welded AA2219 deformed at cryogenic temperatures. Int J Mech Sci. 2024; 274:109221. https://doi.org/10.1016/j.ijmecsci.2024.109221
21. Hussain G, Shehbaz T, Alkahtani M. Investigating impact of in-process cooling mediums on microstructural and mechanical properties of FSWed AA2219 T6 joints. Scientific Reports. 2024; 14(1):29251. https://doi.org/10.1038/s41598-024-80620-x PMid:39587267 PMCid:PMC11589614.
22. Sousa FC, Akhavan-Safar A, Carbas RJ, Marques EA, da Silva LF. A unified strain energy-based fatigue life prediction methodology for composite and metal adhesive joints: Effects of adhesive, geometry and, environment. Composites Prt B: Engineering. 2025; 292:112022. https://doi.org/10.1016/j.compositesb.2024.112022
23. Deng H, Kong J, Liu J, Hu Z, Sun Y, Guo Y, Song L, Yu H. Fatigue reliability analysis methodology based on fatigue life and failure mechanism for arburized gear. Engineering Failure Analysis. 2025; 167:108950. https://doi.org/10.1016/j.engfailanal.2024.108950
24. Qianyu XI, Zhixin ZH, Yue ME, Weiping HU, Qingchun ME. Novel integration of PSO-enhanced damage mechanics and finite element method for predicting medium-low-cycle fatigue life in perforated structures. CJA. 2025; 38(2):103258. https://doi.org/10.1016/j.cja.2024.09.034
25. Omiyale BO, Ogedengbe II, Olugbade TO, Rasheed AA, Ogbeyemi A, Farayibi PK. Cold metal transfer WAAM of aluminum alloys: influence of processing parameters. Int J Adv Manuf Tech. 2025; 136:1967-1987. https://doi.org/10.1007/s00170-024-14989-4
26. Du B, He M, Tang W, Yang X, Yi J, Wang S. Heterogeneity of interfacial microstructure and fracture behaviour of friction plug welds for 2219-T87 AlCu alloy. Materials Characterization. 2025; 222:114864. https://doi.org/10.1016/j.matchar.2025.114864
27. Rao CV, Saranya BL, Prasad GS, Reddy GM, Rao KS. Unveiling the synergistic effect of tool pin profile on AA2219 friction stir welds. J Mater Eng Perform. 2025. https://doi.org/10.1007/s11665-025-10821-6
28. Zhang M, Lai R, Li Y, Wang H, Yang B, Li Y. Influence of protrusion geometry on the microstructure and mechanical properties of AA2219 fabricated by additive friction stir deposition. Progress in additive manufacturing. 2025. https://doi.org/10.1007/s40964-025-01005-8
29. Rajagopal V, Rajendran DK, Muthukumaran S. Multi-objective optimization and characterization of AA2219-T87 and AA6061-T6 dissimilar friction stir welded joints under the effect of copper backing using AUGMECON. Sādhanā. 2024; 49(1):32. https://doi.org/10.1007/s12046-023-02360-4
30. Srinivasan P, RajeshKannan G, Sathiya P. Effect of spherical ball shoulder with square tool pin on the metallurgical and mechanical performance of friction stir welded AA2219-T87 alloy. J Inst Eng India: Series D. 2024. https://doi.org/10.1007/s40033-024-00756-y
31. Mondal S, Raghavendra KG, Panigrahi A, Nayan N, Makineni SK, Suwas S. Effect of Sc addition on evolution of microstructure, texture and strength of high-pressure torsion-processed AA2195 Al-Li alloy. J Mater Sci. 2024; 59(14):5717-5735. https://doi.org/10.1007/s10853-024-09569-6
32. Anderson-Wedge K, Stubblefield G, Zhu N, Long B, Daniewicz SR, Allison P, Sowards J, Rodriguez O, Amaro R. Characterization of the evolution of 2219-T87 aluminum as a function of the friction stir welding process. Int J Fatigue. 2021; 142:105954. https://doi.org/10.1016/j.ijfatigue.2020.105954
33. Manikandan P, Chakravadhanula VS, Rao GS, Manwatkar SK, Murty SN, Sivakumar D, Pant B, Mohan M. Effect

of long-term natural aging on the tensile and fracture properties of aluminum alloy AA2219-T87 parent and weldments at room and cryogenic temperatures. Materials Characterization. 2022; 189:111973. https://doi.org/10.1016/j.matchar.2022.111973

34. Yang B, Lu X, Sun S, Liang SY. Tensile strength prediction and process parameters optimization of FSW thick AA2219-T8 based on ANN-GA. J Braz Soc Mech Sci Eng. 2024; 46(7):388. https://doi.org/10.1007/s40430-024-04962-3
35. Jagadesh KJ, Satyanarayana VV, Rao VV. Entropy weighted TOPSIS taguchi analysis of notch geometry on the fatigue performance of UNS S32760 grade stainless steel. SSRG Int J Mech Eng. 2024; 11(6):82-91. https://doi.org/10.14445/23488360/IJME-V11I6P110.
36. Jagadesh KJ, Satyanarayana VV, Rao VV. Multi-attribute optimization of a ceramic coating on super duplex stainless steel using hybrid taguchi - GTMA - utility technique. IREME. 2024; 18(8):429-437. https://doi.org/10.15866/ireme.v18i8.24959
37. Jagadesh KJ, Satyanarayana VV, Rao VV. Optimization of fatigue response in notched AISI 316L Friction welded joints using a hybrid entropy-VIKOR-taguchi approach. IJETT. 2025; 73(3):265-273. https://doi.org/10.14445/22315381/IJETT-V73I3P120